



**HAL**  
open science

# P- and S-wave velocity of dry, water-saturated, and frozen basalt: Implications for the interpretation of Martian seismic data

Michael Heap

► **To cite this version:**

Michael Heap. P- and S-wave velocity of dry, water-saturated, and frozen basalt: Implications for the interpretation of Martian seismic data. *Icarus*, 2019, 330, pp.11-15. 10.1016/j.icarus.2019.04.020 . hal-02376602

**HAL Id: hal-02376602**

**<https://hal.science/hal-02376602>**

Submitted on 22 Oct 2021

**HAL** is a multi-disciplinary open access archive for the deposit and dissemination of scientific research documents, whether they are published or not. The documents may come from teaching and research institutions in France or abroad, or from public or private research centers.

L'archive ouverte pluridisciplinaire **HAL**, est destinée au dépôt et à la diffusion de documents scientifiques de niveau recherche, publiés ou non, émanant des établissements d'enseignement et de recherche français ou étrangers, des laboratoires publics ou privés.



Distributed under a Creative Commons Attribution - NonCommercial 4.0 International License

1 P- and S-wave velocity of dry, water-saturated, and  
2 frozen basalt: Implications for the interpretation of  
3 Martian seismic data

4

5 Michael J. Heap

6

7 *Géophysique Expérimentale, Institut de Physique de Globe de Strasbourg (UMR*  
8 *7516 CNRS, Université de Strasbourg/EOST), 5 rue René Descartes, 67084*  
9 *Strasbourg cedex, France.*

10

11 Corresponding author: M.J. Heap ([heap@unistra.fr](mailto:heap@unistra.fr))

12

13 **Abstract**

14 The theoretical predictions for the P- and S-wave velocity of [basalt with](#)  
15 [pore spaces filled with gaseous CO<sub>2</sub>, liquid water, or water ice](#) presented herein  
16 could help improve interpretations of the seismic data collected by NASA's  
17 InSight lander, which landed on the Martian surface in November 2018.

18

19 **Keywords:** InSight lander; SEIS; Mars; seismic velocities; basalt

## 20 **Highlights**

21

- 22 • Velocities of porous basalt decrease as a function of increasing porosity
- 23 • Velocities of porous basalt depend on pore aspect ratio
- 24 • Velocities of water ice-saturated basalt are higher than gaseous CO<sub>2</sub>- or  
25 liquid water-saturated basalt
- 26 • Presented modelling could improve interpretations of the seismic data  
27 collected by the InSight lander

28

## 29 **1 Introduction**

30 There is abundant evidence that liquid water existed on the surface of  
31 Mars in its geological past (e.g., Baker, 1979; Carr, 1996; Baker, 2001). However,  
32 the present-day Martian surface is largely dry and water is restricted to polar ice  
33 caps (e.g., Titus et al., 2003; Bibring et al., 2004; Grima et al., 2009) and the  
34 subsurface hydro- and cryosphere (e.g., Fanale et al., 1986; Clifford, 1993;  
35 Boynton et al., 2002; Mitrofanov et al., 2003; Mellon et al., 2004; Orosei et al.,  
36 2018). Since the surface temperature of Mars ranges from -150 to 20 °C,  
37 subsurface water exists as water ice or liquid water, varying with, amongst other  
38 factors, space (i.e. latitude) and time (i.e. seasonal variations) (e.g., Fanale et al.,  
39 1986; Bandfield, 2007).

40 NASA's InSight lander (Banerdt et al., 2013) touched down on the Martian  
41 surface on 26 November 2018. One of the aims of the InSight mission is to better  
42 understand the interior of Mars using a seismometer (Seismic Experiment for  
43 Interior Structure, SEIS; Panning et al., 2015; 2017). Since laboratory  
44 measurements and theoretical predictions show that elastic wave velocities for

45 rock can differ depending on whether the rock is dry or saturated with either  
46 liquid water or water ice (e.g., O'Connell and Budiansky, 1974; Toksöz et al.,  
47 1976; Kahraman, 2007), the influence of saturation state on the P- and S-wave  
48 velocity of crustal rocks is therefore of interest to those tasked with using  
49 seismic data collected by SEIS to interpret the structure and physical properties  
50 (e.g., porosity) of the shallow Martian subsurface (the brittle lithosphere) and to  
51 locate marsquakes and impacts. Due to the paucity of laboratory measurements  
52 and theoretical predictions, the P- and S-wave velocity of dry, water-saturated,  
53 and frozen basalt—the most representative rock type of the Martian crust  
54 (McSween et al., 2009)—are estimated herein as a function of porosity and pore  
55 shape using scattering theory.

56

## 57 **2 Theory**

58 Porous basalt, a solid groundmass that hosts pores (e.g., Saar and Manga,  
59 1999; Al-Harhi et al., 1999; Bubeck et al., 2017), can be approximated by an  
60 equivalent homogeneous medium for wavelengths that are much longer than the  
61 characteristic pore size. Assuming that the pores (represented by spheres and  
62 oblate spheroids) are randomly distributed and that the medium is isotropic,  
63 scattering theory can be used to calculate the elastic wave velocities of the  
64 equivalent medium (Kuster and Toksöz, 1974; Toksöz et al., 1976). The  
65 equivalent bulk modulus,  $K^*$ , equivalent shear modulus,  $\mu^*$ , and equivalent  
66 density,  $\rho^*$ , of the equivalent homogeneous medium are given by (Kuster and  
67 Toksöz, 1974; Toksöz et al., 1976):

68

69 
$$\frac{K^* - K}{3K^* + 4\mu} = \frac{1}{3} \cdot c \cdot \frac{K' - K}{3K + 4\mu} T_{iijj}, \quad (1)$$

70

71 
$$\frac{\mu^* - \mu}{6\mu^*(K + 2\mu) + \mu(9K + 8\mu)} = c \frac{(\mu' - \mu)}{25\mu(3K + 4\mu)} \left[ T_{ijij} - \frac{1}{3} T_{iijj} \right], \quad (2)$$

72

73 
$$\rho^* = \rho(1 - c) + c\rho'. \quad (3)$$

74

75 Where  $K$ ,  $\mu$ , and  $\rho$ , are the bulk modulus, shear modulus, and density of the solid  
 76 groundmass, respectively, and  $K'$ ,  $\mu'$ , and  $\rho'$  are the bulk modulus, shear  
 77 modulus, and density of the pore-filling **medium**, respectively.  $T_{iijj}$  and  $T_{ijij}$  are  
 78 scalar quantities that depend on the aspect ratio of the pores and the elastic  
 79 properties of the groundmass and pore-filling **medium** (Kuster and Toksöz,  
 80 1974; Toksöz et al., 1976) and are given by:

81

82 
$$T_{iijj} = \frac{3F_1}{F_2}, \quad (4)$$

83

84 
$$T_{ijij} - \frac{1}{3} T_{iijj} = \frac{2}{F_3} + \frac{1}{F_4} + \frac{F_4 F_5 + F_6 F_7 - F_8 F_9}{F_2 F_4}. \quad (5)$$

85

86 Where:

87

88 
$$F_1 = 1 + A \left[ \frac{3}{2} (g + \phi) - R \left( \frac{3}{2} g + \frac{5}{2} \phi - \frac{4}{3} \right) \right], \quad (6)$$

$$\begin{aligned}
89 \quad F_2 &= 1 + A \left[ 1 + \frac{3}{2}(g + \phi) - \frac{R}{2}(3g + 5\phi) \right] + B(3 - 4R) \\
90 \quad &+ \frac{A}{2}(A + 3B)(3 - 4R)[g + \phi - R(g - \phi + 2\phi^2)], \quad (7)
\end{aligned}$$

$$91 \quad F_3 = 1 + \frac{A}{2} \left[ R(2 - \phi) + \frac{(1 + \alpha^2)}{\alpha^2} g(R - 1) \right], \quad (8)$$

$$92 \quad F_4 = 1 + \frac{A}{4} [3\phi + g - R(g - \phi)], \quad (9)$$

$$93 \quad F_5 = A \left[ R \left( g + \phi - \frac{4}{3} \right) - g \right] + B\phi(3 - 4R), \quad (10)$$

$$94 \quad F_6 = 1 + A[1 + g - R(g + \phi)] + B(1 - \phi)(3 - 4R), \quad (11)$$

$$95 \quad F_7 = 2 + \frac{A}{4} [9\phi + 3g - R(5\phi + 3g)] + B\phi(3 - 4R), \quad (12)$$

$$96 \quad F_8 = A \left[ 1 - 2R + \frac{g}{2}(R - 1) + \frac{\phi}{2}(5R - 3) \right] + B(1 - \phi)(3 - 4R), \quad (13)$$

$$97 \quad F_9 = A[g(R - 1) - R\phi] + B\phi(3 - 4R), \quad (14)$$

$$98 \quad A = \frac{\mu'}{\mu} - 1, \quad (15)$$

$$99 \quad B = \frac{1}{3} \left( \frac{K'}{K} - \frac{\mu'}{\mu} \right), \quad (16)$$

$$100 \quad R = \frac{3\mu}{3K + 4\mu}, \quad (17)$$

$$101 \quad \phi = \frac{\alpha}{(1 - \alpha^2)^{3/2}} [\cos^{-1} \alpha - \alpha(1 - \alpha^2)^{1/2}], \quad (18)$$

$$102 \quad g = \frac{\alpha^2}{1 - \alpha^2} (3\phi - 2). \quad (19)$$

103

104 The P-wave velocity,  $V_p^*$ , and S-wave velocity,  $V_s^*$ , of the equivalent homogeneous

105 medium can then be calculated using the following expressions (Kuster and

106 Toksöz, 1974; Toksöz et al., 1976):

107

108 
$$V_p^* = \left[ \frac{K^* + 4/3 \mu^*}{\rho^*} \right]^{1/2}, \quad (20)$$

109

110 
$$V_s^* = \left[ \frac{\mu^*}{\rho^*} \right]^{1/2}. \quad (21)$$

111

### 112 **3 Model set up and considerations**

113 The equivalent bulk modulus, equivalent shear modulus, and equivalent  
114 density of porous basalt saturated with liquid water, water ice, and gaseous CO<sub>2</sub>  
115 (the most abundant molecule in the present-day Martian atmosphere; Owen et  
116 al., 1977) were determined for pore aspect ratios from 0.1 to 1 (since the aspect  
117 ratio of pores within basalt on Earth can vary significantly; e.g., Bubeck et al.,  
118 2017) and for porosities from 0 to 0.2 (since the porosity of basalt on Earth can  
119 also vary; e.g., Saar and Manga, 1999) using Equations 1, 2, and 3 and the values  
120 provided in Table 1. The P- and S-wave velocities of these equivalent media were  
121 then calculated using Equations 20 and 21, respectively. The values in Table 1  
122 were simply chosen to explore the range of possible pore fluid properties in the  
123 Martian subsurface. I highlight here that, for example, the density of CO<sub>2</sub>  
124 increases from 1.8 to 2.3 kg/m<sup>3</sup> as temperature is decreased from 20 to -40 °C  
125 (at a pressure of 0.1 MPa). CO<sub>2</sub> will be a liquid, with a density close to liquid  
126 water, at ~0 °C when, for example, the pressure is higher than a few megapascals  
127 and at ~-60 °C when the pressure is higher than ~1 MPa. CO<sub>2</sub> will be a solid at  
128 temperatures ≥ ~-80 °C. Indeed, there is evidence of frozen CO<sub>2</sub> on the surface of  
129 Mars and its presence is inferred for the Martian subsurface (e.g., Mitrofanov et  
130 al., 2003). Although the density of frozen CO<sub>2</sub> is higher than that of water ice

131 (frozen CO<sub>2</sub> has a density between 1400 and 1600 kg/m<sup>3</sup> at ~-80 °C and water  
132 ice has a density of 980 kg/m<sup>3</sup> at ~-40 °C; Table 1), their bulk moduli, for  
133 example, are very similar (Table 1; Liu, 1984). Therefore, the estimated  
134 velocities for rock saturated with liquid water may approximate those for rock  
135 saturated with liquid CO<sub>2</sub>, and the estimated velocities for water ice-saturated  
136 rock may approximate those for rock saturated with solid (i.e. frozen) CO<sub>2</sub>. I also  
137 highlight that liquid water and water ice on Mars could contain salts (e.g., Clark  
138 and van Hart, 1981; Vaniman et al., 2004; Zorzano et al., 2009; Stillman and  
139 Grimm, 2011) that would serve to slightly increase density (the density of  
140 seawater at 0.1 MPa, for example, varies between 1020 and 1029 kg/m<sup>3</sup>) and  
141 lower the freezing point (salt solutions at the point of saturation will freeze at ~-  
142 20 °C). I further highlight that the densities of liquid water and water ice do not  
143 increase significantly as temperature is decreased. For example, the density of  
144 liquid water increases from 998.2 kg/m<sup>3</sup> at 20 °C to 999.8 kg/m<sup>3</sup> just above the  
145 freezing temperature. For simplicity, therefore, a water density of 1000 kg/m<sup>3</sup>  
146 was adopted herein (Table 1).  
147

	Density (kg/m <sup>3</sup> )	Bulk modulus (Pa)	Shear modulus (Pa)
Solid (i.e. pore-free) basalt groundmass	2900	$8.0 \times 10^{10}$	$4.0 \times 10^{10}$
Liquid water (20 °C)	1000	$2.2 \times 10^9$	0



Water ice (-40 °C)	980	$8.1 \times 10^9$	$3.7 \times 10^9$
Gaseous CO <sub>2</sub> (20 °C)	1.8	$1.0 \times 10^5$	0

148

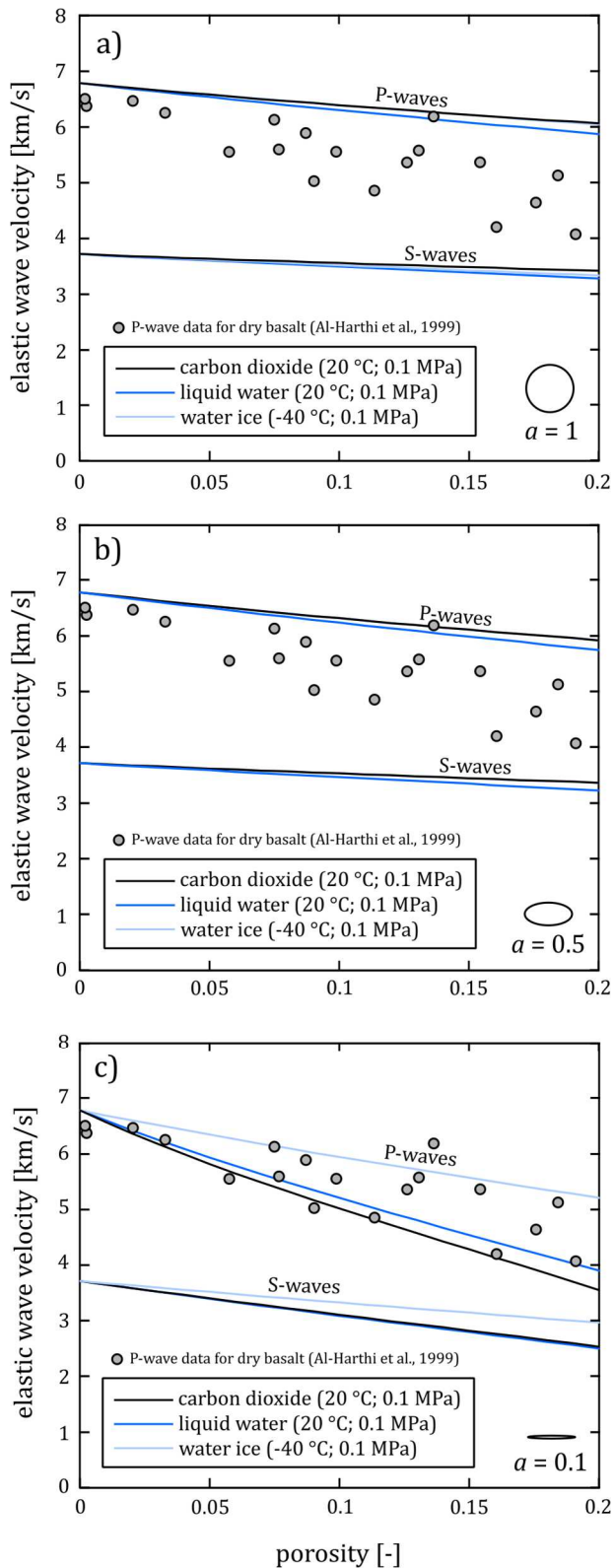
149 **Table 1.** Density, bulk modulus, and shear modulus for the solid groundmass of  
150 the basalt and the three pore fluids. Solid properties for basalt estimated using  
151 data from Christensen (1972). Properties of water ice at -40 °C were taken from  
152 Toksöz et al. (1976). Properties of liquid water and CO<sub>2</sub> are for a pressure of 0.1  
153 MPa and a temperature of 20 °C.

154

#### 155 **4 Results**

156 The P- and S-wave velocity of basalt saturated with gaseous CO<sub>2</sub>, liquid  
157 water, and water ice are plotted in Figure 1 as a function of porosity. Figures 1a,  
158 1b, and 1c show examples of the modelled curves for pore aspect ratios of 1 (i.e.  
159 a perfect sphere), 0.5, and 0.1, respectively.

160



161

162 **Figure 1.** Elastic wave velocity (P- and S-wave velocity) of basalt as a function of  
 163 porosity and saturating fluid/medium, calculated using scattering theory (see  
 164 main text for details). (a) Elastic wave velocities for a basalt containing pores

165 with an aspect ratio of unity. (b) Elastic wave velocities for a basalt containing  
166 pores with an aspect ratio of 0.5. (c) Elastic wave velocities for a basalt  
167 containing pores with an aspect ratio of 0.1. The modelled curves are plotted  
168 alongside laboratory-measured P-wave velocity data for dry porous basalt (data  
169 from Al-Harhi et al., 1999).

170

171 The modelling shows that there are only small differences between the P-  
172 and S-wave velocities for basalts with pore aspect ratios above 0.4 (Figures 1a  
173 and 1b show modelled results for pore aspect ratios of 1 and 0.5, respectively).  
174 Below a pore aspect ratio of 0.4, the P- and S-wave velocities for basalt  
175 containing water ice within the pores are higher than those containing gaseous  
176 CO<sub>2</sub> and liquid water (Figure 1c shows modelled results for a pore aspect ratio  
177 0.1).

178 The example shown in Figure 1c (pore aspect ratio = 0.1) shows that the  
179 P-wave velocity of basalt with pores containing water ice at a porosity of 0.2 can  
180 be more than 1 km/s higher than basalt containing liquid water, and almost 1.5  
181 km/s higher than basalt containing gaseous CO<sub>2</sub>. The S-wave velocity of basalt  
182 containing water ice is about 0.5 km/s higher than basalt containing either liquid  
183 water or gaseous CO<sub>2</sub>, and the P-wave velocity of the water-saturated basalt is  
184 higher, by about 0.5 km/s, than the basalt containing gaseous CO<sub>2</sub>, although their  
185 S-wave velocities are essentially identical (Figure 1c).

186

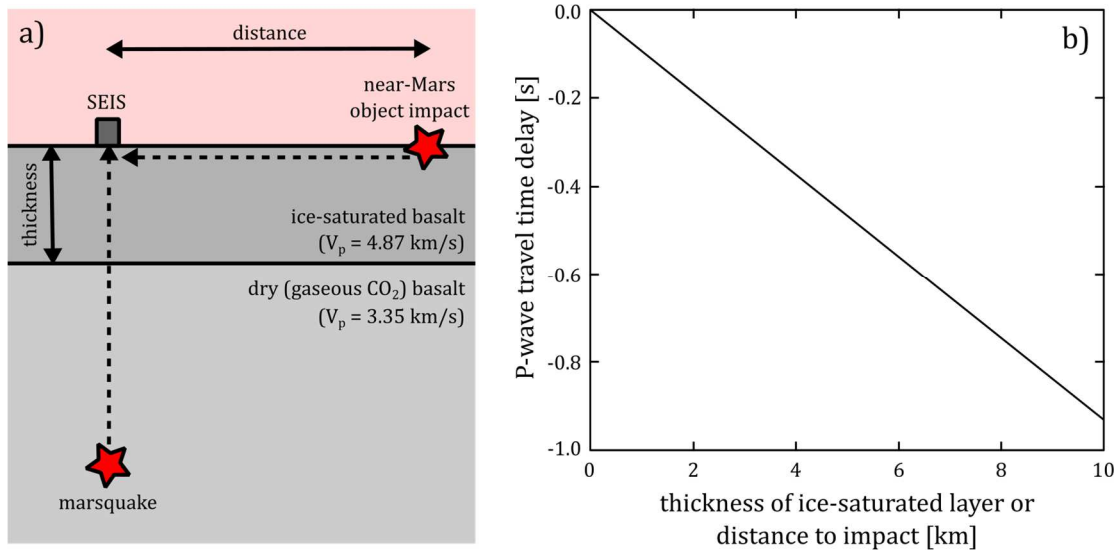
## 187 **5 Discussion, implications, and conclusions**

188 Theoretical calculations, based on scattering theory, show that the P- and  
189 S-wave velocity of frozen basalt (i.e. basalt containing water ice-filled pores) is

190 higher than dry (containing gaseous CO<sub>2</sub>) and water-saturated basalt when the  
191 pore aspect ratio is low (for the range of porosity values tested herein; Figure 1).  
192 These predictions are in accordance with previous observations of and  
193 theoretical predictions for ice- and water-saturated sandstone, limestone, and  
194 granite (Toksöz et al., 1976). The modelled curves of Figure 1 are plotted  
195 alongside laboratory-measured P-wave velocities for dry porous basalt (from  
196 Saudi Arabia; data from Al-Harhi et al., 1999). Not only is the P-wave velocity of  
197 the basalt with a very low porosity (a porosity of 0.002) close to the modelled  
198 curves, validating the chosen P-wave velocity for porosity-free basalt (Table 1),  
199 but the decrease as a function of porosity also closely matches that of the  
200 modelling. The comparison between these data and the modelled curves  
201 suggests that the pores within the basalt have an aspect ratio between 1.0 and  
202 0.1 (Figure 1). Indeed, Al-Harhi et al. (1999) note that the pores in these basalts  
203 “vary in shape between being spherical and irregular, but are generally  
204 spherical”.

205         Since low aspect ratio voids (i.e. elongated pores and fractures, the latter  
206 of which typically have an aspect ratio less than 0.01) may be commonplace in a  
207 potentially highly fractured Martian crust (e.g., Carr, 1974; MacKinnon and  
208 Tanaka, 1989; Rodríguez et al., 2005; Heap et al., 2017), and estimates for the  
209 depth of the base of the cryosphere are 2.3 and 6.5 km for the equator and poles,  
210 respectively (Clifford, 1993), it is therefore not unreasonable to expect  
211 differences in elastic wave velocities in the Martian subsurface solely as a result  
212 of the saturating fluid/medium. To assess the influence of a higher-velocity layer  
213 on the measured travel times from impacts and marsquakes, I present the results  
214 of some back-of-the-envelope calculations in Figure 2.

215



216

217 **Figure 2.** Back-of-the-envelope P-wave travel time delay calculations. (a)  
218 Schematic showing the simple model setup. (b) P-wave travel time delay (the  
219 difference in travel time between a Martian subsurface with and without a  
220 higher-velocity ice-saturated layer) as a function of the thickness of the ice-  
221 saturated layer (for marsquakes) or the distance to impact (for impacts).

222

223 The simple model assumes a simple subsurface structure consisting of an  
224 ice-saturated basalt layer above a dry basalt layer, both homogenous in terms of  
225 their [intra-layer](#) seismic velocities, a flat Martian surface, and [direct \(i.e. non-](#)  
226 [reflected\)](#) raypaths (Figure 2a). These calculations are designed to test the  
227 influence of an ice-saturated layer on the travel time delay in isolation. I highlight  
228 that there are other factors, not considered here (Figure 2), such as rock type  
229 (e.g., Lesage et al., 2018) and hydrothermal alteration (e.g., Pola et al., 2012;  
230 Mordensky et al., 2018) that are known to influence the seismic velocities of  
231 volcanic rocks. The P-wave velocities of the layers [within the model](#) are assumed  
232 to be 4.87 and 3.35 km/s for the ice-saturated and dry basalt layers, respectively

233 (the P-wave velocities for at porosity of 0.2 and a pore aspect ratio of 0.1; Figure  
234 1c), and therefore the travel time delay presented in Figure 2b could be  
235 considered the maximum travel time delay (i.e., the travel time delays presented  
236 here would be reduced if the porosities of the considered rock layers were  
237 reduced, for example). These simple calculations show that the travel time delay  
238 could be as much at 0.5 s for an impact even 5 km from the InSight lander,  
239 resulting in a location error of about 2 km. Based on these back-of-the-envelope  
240 calculations, the presence, and thickness, of a high-velocity ice-saturated layer  
241 could be an important consideration when using data collected by SEIS to assess  
242 the structure of the shallow Martian subsurface (the brittle lithosphere) and to  
243 locate marsquakes and impacts.

244 I note that the P- and S-wave velocity estimates provided herein do not  
245 take depth into account, which will serve to decrease porosity (e.g., Clifford,  
246 1993; Wilson and Head, 1994; Heap et al., 2017) and therefore increase elastic  
247 wave velocities. However, the analysis presented herein shows that differences  
248 in P-wave velocity would be observed, in the case of low aspect ratio pores  
249 (Figure 1c), even if porosity is reduced to between 0.02-0.05, the porosity  
250 predicted for depths between 6 and 10 km (Clifford, 1993). Finally, I highlight  
251 that the small changes in pore fluid properties associated with differences in  
252 temperature (e.g., the temperature of liquid water on Mars may vary from 20 to  
253 0.5 °C) and/or salinity (e.g., liquid water on Mars is likely to contain salts; Clark  
254 and van Hart, 1981; Vaniman et al., 2004; Zorzano et al., 2009; Stillman and  
255 Grimm, 2011) do not significantly influence the predictions presented in Figure  
256 1. For example, the modelled curves for rock containing liquid water at a

257 temperature of 20 °C superimpose those for rock containing liquid water at 0.5  
258 °C.

259 The predictions presented herein, that elastic wave velocity depends on  
260 the void fraction and the nature of the fluid/medium within those pores, may  
261 help improve assessments of the structure of the shallow subsurface (brittle  
262 lithosphere) of Mars and place more accurate bounds on the locations of  
263 marsquake hypocentres and surface impacts detected by the SEIS instrument on  
264 the InSight lander (e.g., Teanby and Wookey, 2011). Further, if a saturating-  
265 medium is assumed, the presented modelling can be used to provide estimates of  
266 the physical properties (e.g., porosity) of the Martian subsurface. Seismic  
267 reflection and transmission coefficients (e.g., Ben-Menahem and Singh, 2012),  
268 useful for a wide range of seismological applications, could also be determined  
269 using the modelling described herein. Finally, if this method can be used to  
270 detect subsurface bodies of liquid water, it could be used to identify potentially  
271 habitable sites on Mars, or as an independent check for sites identified using  
272 other methods, such as radar (e.g., Orosei et al., 2018).

273

#### 274 **Acknowledgements**

275 The author thanks a Prix d'Espoirs grant awarded by the University of  
276 Strasbourg. The author also acknowledges inspiring conversations with Olivier  
277 Lengliné, Paul Byrne, Sami Mikhail, Claire Cousins, Peter Grindrod, Jamie  
278 Farquharson, and Luke Griffiths. The comments of two reviewers helped  
279 improve this manuscript.

280

#### 281 **Competing interests**

282 The author declares no competing interests.

283

## 284 **References**

- 285 Al-Harthi, A. A., Al-Amri, R. M., & Shehata, W. M. (1999). The porosity and engineering  
286 properties of vesicular basalt in Saudi Arabia. *Engineering Geology*, 54(3-4), 313-  
287 320.
- 288 Baker, V. R. (1979). Erosional processes in channelized water flows on Mars. *Journal of*  
289 *Geophysical Research: Solid Earth*, 84(B14), 7985-7993.
- 290 Baker, V. R. (2001). Water and the Martian landscape. *Nature*, 412(6843), 228.
- 291 Bandfield, J. L. (2007). High-resolution subsurface water-ice distributions on  
292 Mars. *Nature*, 447(7140), 64.
- 293 Banerdt, W. B., Smrekar, S., Lognonné, P., Spohn, T., Asmar, S. W., Banfield, D., ... &  
294 Giardini, D. (2013, March). InSight: a discovery mission to explore the interior of  
295 Mars. In *Lunar and planetary science conference* (Vol. 44, p. 1915).
- 296 [Ben-Menahem, A., & Singh, S. J. \(2012\). Seismic waves and sources. Springer Science &](#)  
297 [Business Media.](#)
- 298 Bibring, J. P., Langevin, Y., Poulet, F., Gendrin, A., Gondet, B., Berthé, M., ... & Moroz, V.  
299 (2004). Perennial water ice identified in the south polar cap of  
300 Mars. *Nature*, 428(6983), 627.
- 301 Boynton, W. V., Feldman, W. C., Squyres, S. W., Prettyman, T. H., Brückner, J., Evans, L. G.,  
302 ... & Englert, P. A. J. (2002). Distribution of hydrogen in the near surface of Mars:  
303 Evidence for subsurface ice deposits. *science*, 297(5578), 81-85.
- 304 Bubeck, A., Walker, R. J., Healy, D., Dobbs, M., & Holwell, D. A. (2017). Pore geometry as a  
305 control on rock strength. *Earth and Planetary Science Letters*, 457, 38-48.
- 306 Carr, M. H. (1974). Tectonism and volcanism of the Tharsis region of Mars. *Journal of*  
307 *Geophysical Research*, 79(26), 3943-3949.
- 308 Carr, M. H. (1996). Water erosion on Mars and its biologic  
309 implications. *Endeavour*, 20(2), 56-60.
- 310 Clark, B. C., & Van Hart, D. C. (1981). The salts of Mars. *Icarus*, 45(2), 370-378.
- 311 Clifford, S. M. (1993). A model for the hydrologic and climatic behavior of water on  
312 Mars. *Journal of Geophysical Research: Planets*, 98(E6), 10973-11016.
- 313 Fanale, F. P., Salvail, J. R., Zent, A. P., & Postawko, S. E. (1986). Global distribution and  
314 migration of subsurface ice on Mars. *Icarus*, 67(1), 1-18.
- 315 Grima, C., Kofman, W., Mougnot, J., Phillips, R. J., Hérique, A., Biccari, D., ... & Cutigni, M.  
316 (2009). North polar deposits of Mars: Extreme purity of the water ice. *Geophysical*  
317 *Research Letters*, 36(3).
- 318 Heap, M. J., Byrne, P. K., & Mikhail, S. (2017). Low surface gravitational acceleration of  
319 Mars results in a thick and weak lithosphere: Implications for topography,  
320 volcanism, and hydrology. *Icarus*, 281, 103-114.
- 321 Kahraman, S. (2007). The correlations between the saturated and dry P-wave velocity of  
322 rocks. *Ultrasonics*, 46(4), 341-348.
- 323 Kuster, G. T., & Toksöz, M. N. (1974). Velocity and attenuation of seismic waves in two-  
324 phase media: Part I. Theoretical formulations. *Geophysics*, 39(5), 587-606.
- 325 [Lesage, P., Heap, M. J., & Kushnir, A. \(2018\). A generic model for the shallow velocity](#)  
326 [structure of volcanoes. Journal of Volcanology and Geothermal Research](#), 356,  
327 [114-126.](#)
- 328 [Liu, L. G. \(1984\). Compression and phase behavior of solid CO2 to half a megabar. Earth](#)  
329 [and Planetary Science Letters](#), 71(1), 104-110.



330 MacKinnon, D. J., & Tanaka, K. L. (1989). The impacted Martian crust: Structure,  
331 hydrology, and some geologic implications. *Journal of Geophysical Research: Solid*  
332 *Earth*, 94(B12), 17359-17370.

333 McSween, H. Y., Taylor, G. J., & Wyatt, M. B. (2009). Elemental composition of the Martian  
334 crust. *Science*, 324(5928), 736-739.

335 Mellon, M. T., Feldman, W. C., & Prettyman, T. H. (2004). The presence and stability of  
336 ground ice in the southern hemisphere of Mars. *Icarus*, 169(2), 324-340.

337 Mitrofanov, I. G., Zuber, M. T., Litvak, M. L., Boynton, W. V., Smith, D. E., Drake, D., ... &  
338 Saunders, R. S. (2003). CO<sub>2</sub> snow depth and subsurface water-ice abundance in  
339 the northern hemisphere of Mars. *Science*, 300(5628), 2081-2084.

340 [Mordensky, S. P., Villeneuve, M. C., Kennedy, B. M., Heap, M. J., Gravley, D. M.,  
341 Farquharson, J. I., & Reuschlé, T. \(2018\). Physical and mechanical property  
342 relationships of a shallow intrusion and volcanic host rock, Pinnacle Ridge, Mt.  
343 Ruapehu, New Zealand. \*Journal of Volcanology and Geothermal Research\*, 359, 1-  
344 20.](#)

345 O'Connell, R. J., & Budiansky, B. (1974). Seismic velocities in dry and saturated cracked  
346 solids. *Journal of Geophysical Research*, 79(35), 5412-5426.

347 Orosei, R., Lauro, S. E., Pettinelli, E., Cicchetti, A., Coradini, M., Cosciotti, B., ... & Soldovieri,  
348 F. (2018). Radar evidence of subglacial liquid water on Mars. *Science*, 361(6401),  
349 490-493.

350 Owen, T., Biemann, K., Rushneck, D. R., Biller, J. E., Howarth, D. W., & Lafleur, A. L. (1977).  
351 The composition of the atmosphere at the surface of Mars. *Journal of Geophysical*  
352 *research*, 82(28), 4635-4639.

353 Panning, M. P., Beucler, É., Drilleau, M., Mocquet, A., Lognonné, P., & Banerdt, W. B.  
354 (2015). Verifying single-station seismic approaches using Earth-based data:  
355 Preparation for data return from the InSight mission to Mars. *Icarus*, 248, 230-  
356 242.

357 Panning, M. P., Lognonné, P., Banerdt, W. B., Garcia, R., Golombek, M., Kedar, S., ... &  
358 Weber, R. (2017). Planned products of the Mars structure service for the InSight  
359 mission to Mars. *Space Science Reviews*, 211(1-4), 611-650.

360 [Pola, A., Crosta, G., Fusi, N., Barberini, V., & Norini, G. \(2012\). Influence of alteration on  
361 physical properties of volcanic rocks. \*Tectonophysics\*, 566, 67-86.](#)

362 Rodríguez, J. A. P., Sasaki, S., Dohm, J. M., Tanaka, K. L., Strom, B., Kargel, J., ... & Komatsu,  
363 G. (2005). Control of impact crater fracture systems on subsurface hydrology,  
364 ground subsidence, and collapse, Mars. *Journal of Geophysical Research:*  
365 *Planets*, 110(E6).

366 Saar, M. O., & Manga, M. (1999). Permeability-porosity relationship in vesicular  
367 basalts. *Geophysical Research Letters*, 26(1), 111-114.

368 Stillman, D. E., & Grimm, R. E. (2011). Dielectric signatures of adsorbed and salty liquid  
369 water at the Phoenix landing site, Mars. *Journal of Geophysical Research:*  
370 *Planets*, 116(E9).

371 Teanby, N. A., & Wookey, J. (2011). Seismic detection of meteorite impacts on  
372 Mars. *Physics of the Earth and Planetary Interiors*, 186(1-2), 70-80.

373 Titus, T. N., Kieffer, H. H., & Christensen, P. R. (2003). Exposed water ice discovered near  
374 the south pole of Mars. *Science*, 299(5609), 1048-1051.

375 Toksöz, M. N., Cheng, C. H., & Timur, A. (1976). Velocities of seismic waves in porous  
376 rocks. *Geophysics*, 41(4), 621-645.

377 Vaniman, D. T., Bish, D. L., Chipera, S. J., Fialips, C. I., Carey, J. W., & Feldman, W. C. (2004).  
378 Magnesium sulphate salts and the history of water on Mars. *Nature*, 431(7009),  
379 663.

380 Wilson, L., & Head, J. W. (1994). Mars: Review and analysis of volcanic eruption theory  
381 and relationships to observed landforms. *Reviews of Geophysics*, 32(3), 221-263.

382 Zorzano, M. P., Mateo-Martí, E., Prieto-Ballesteros, O., Osuna, S., & Renno, N. (2009).  
383 Stability of liquid saline water on present day Mars. *Geophysical Research*  
384 *Letters*, 36(20).